Nanoscale

Accepted Manuscript

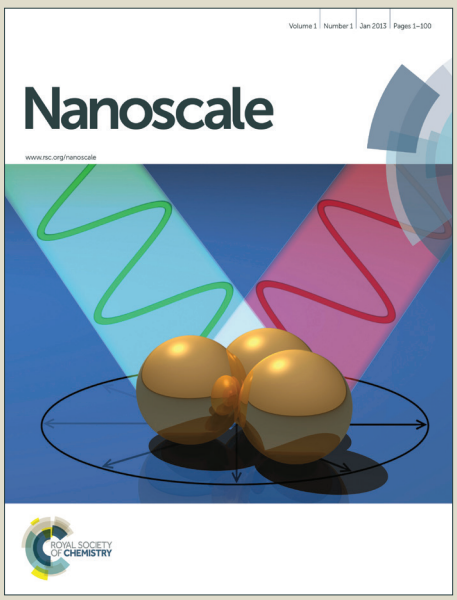

ROYAL SOCIETY OF CHEMISTRY

www.rsc.org/nanoscale

Journal Name

RSCPublishing

COMMUNICATION

Copper metal-organic framework nanocrystal for plane effect nonenzymatic electro-catalytic glucose

Cite this: DOI: 10.1039/x0xx00000x

Yuanying Liu,[a] Youjuan Zhang,[a] Jing Chen,[a] and Huan Pang*[a, b]

Received 00th January 2012,
Accepted 00th January 2012

DOI: 10.1039/x0xx00000x

www.rsc.org/

$[Cu_3(btc)_2]$ nanocrystals with different shapes (nanocube, truncated cube, cuboctahedron, and octahedron) are the firstly demonstrated nanocrystal plane dependent nonenzymatic electro-catalytic glucose. From electrochemical results, the obtained $[Cu_3(btc)_2]$ nanocube modified electrode shows the best nonenzymatic electro-catalytic glucose activity. Interestingly, with the decreasing of {100} crystal planes from cubes to octahedra, the nonenzymatic electro-catalytic activity changes from the high sensitive to general.

Introduction

Designed metal–organic frameworks (MOFs) have shown promising applications in catalysis, separation, gas storage, biomedical imaging, and drug delivery.[1–6] Recently, several investigators have begun exploring the potential of MOFs as chemical sensors. The exceptional tunability of MOF structures and properties should constitute an important advantage over other conventional chemo-sensory materials. Therefore, MOF-based sensors have significant potential for development of powerful analytical techniques for the determination of biomolecules in clinical, environmental, and industrial applications.[6-10]

MOFs have rarely been utilized for conductivity-based sensing applications due to the majority of MOFs are insulating materials. With the development of nanoscience and nanotechnology, nanostructured MOFs show great application potential in electrochemical sensing, for example, Mao et al. designed an integrated dehydrogenase-based electrochemical biosensor by using ZIFs-70 as the matrix for the in-vivo measurement of neurochemicals. [11] Wei and Mao et al. reported Cu-MOF-modified electrodes for oxygen reduction reaction. [12] Xu et al. reported the exploitation of a novel Cu-MOF as electrocatalysts for H_2O_2 oxidation.[13] Bagheri et al. reported Au-SH-SiO_2@Cu-MOF showed good electrocatalytic activity toward the oxidation of L-cysteine, and hydrazine.[14, 15] Wang et al reported the water oxidation electrocatalysis by a zeolitic imidazolate framework.[16]

The conspicuous physical–chemical properties of nanostructures, as we all know, are sensitively correlated to their surface crystal planes, which makes it very important to control the synthesis of the nanomaterials to provide different crystal planes for crystal plane–property investigations, especially under the same or similar conditions.[17-21] $[Cu_3(btc)_2]$ (btc^{3-} = benzene-1,3,5-tricarboxylate), known as HKUST-1, has been one of the first MOF compounds studied extensively in the last decade due to its potential applications in gas sorption, storage and separation.[22] There are many strategies that have been reported for the synthesis of nanosized $[Cu_3(btc)_2]$, including solvothermal,[23] ultrasonic,[24] microwave-assisted,[25] mechanochemical methods and solvothermal synthesis.[26-29] Recently, a rapid synthesis of nanostructured $[Cu_3(btc)_2]$ with high yields at room temperature has been reported by Sun et al.[30] Despite the large number of papers published on $[Cu_3(btc)_2]$, little effort has been made on the exploitation of nanostructured $[Cu_3(btc)_2]$ as nonenzymatic electrocatalysts for electrochemical sensors.

This work describes the first demonstration the nanocrystal plane dependent nonenzymatic electro-catalytic glucose of $[Cu_3(btc)_2]$ nanocrystals. We provide a facile and rapid method to synthesize morphology- and size-controlled nano/microscale $[Cu_3(btc)_2]$ by the modified method of Sun et al.[30] $[Cu_3(btc)_2]$ nanocubes, truncated cubes, cuboctahedrons and octahedrons have been successfully obtained. Interestingly, the obtained $[Cu_3(btc)_2]$ nanocube with 6{100} crystal plane modified electrode shows the best electro-catalytic glucose oxidation activity of four as-prepared samples. Additonally,

with the crystal plane changing of the $[Cu_3(btc)_2]$ nanocrystals from the cubic to the octahedral, the nonenzymatic electro-catalytic glucose property changes from high sensitivity to general response.

Results and discussion

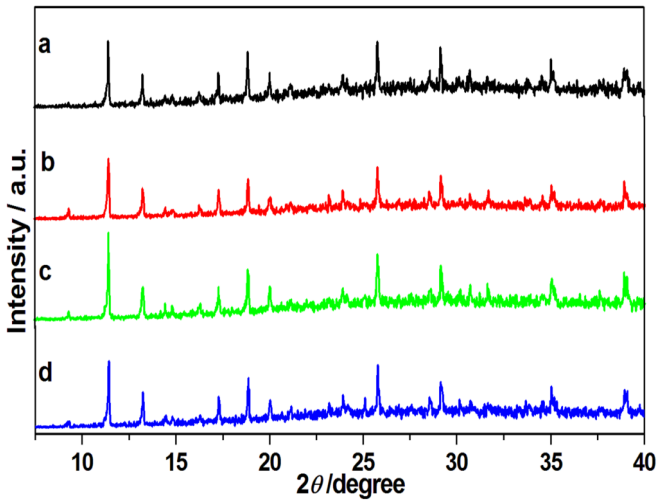

Figure 1 XRD patterns of as-prepared samples obtained from 0.15 mL 0.1 M $Cu(NO_3)_2$ and 0.1 mL 0.1 M btc sodium salt with different amounts of CTAB (0, 0.005 M, 0.01 M, and 0.1 M, the corresponding product is denoted by S1, S2, S3, and S4 respectively); a) S1, b) S2, c) S3, and d) S4.

The $[Cu_3(btc)_2]$ nanocubes, truncated cubes, cuboctahedrons and octahedrons have been successfully obtained by a low-cost chemical precipitation with the addition of the surfactant cetyltrimethylammonium bromide (CTAB) at room temperature (See in experimental section). **Figure 1** shows XRD patterns of as-prepared samples with different morphologies. In Figure 1, all the characteristic diffraction peaks of as-prepared samples are identified, and all the products are pure-phase $[Cu_3(btc)_2]$ powders, which is the same as Sun et al's results.[30] There are no obvious different peaks among the four nanostructured materials.

Figure 2a, b show the product (Denoted by **S1**) with cubic shapes obtained without the addition of CTAB. In addition, the nanocubic crystal always has 6 {100} facets. The average size of S1 is about 220 nm in Figure 2b. When increasing the concentration of CTAB to 0.005 M, the morphology of the as-prepared sample (Denoted by **S2**) changes to truncated cubes consisting of 6 {100} and 8 {111} facets in Figure 2c, but the size of S2 remains about 250 nm (Figure 2d). When the concentration of CTAB to 0.01 M is further increased, the product (Denoted by **S3**) facets of {111} get larger in Figure 2f, and thus cubeoctahedrons form with average sizes of about 260 nm in Figure 2f. When the concentration of CTAB is further increased to 0.1 M, the {100} facets disappear and octahedral nanoparticles (Denoted by **S4**) of about 360 nm in size are obtained (Figure 2g, h).

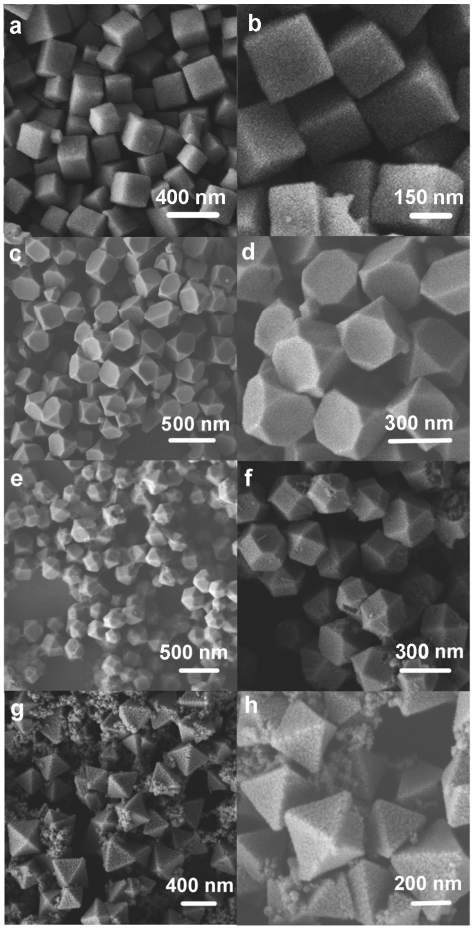

Figure 2 FE-SEM images of as-prepared samples, a, b) S1, c, d) S2, e, f) S3, and g, h) S4.

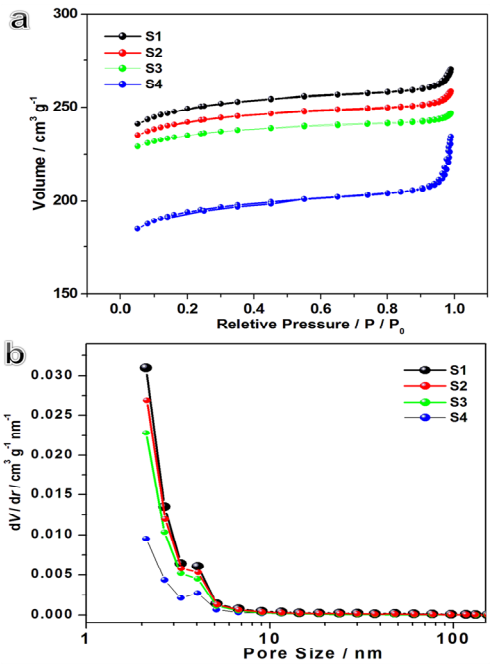

Figure 3 a) Adsorption and desorption isotherms for nitrogen (at 77 K) of as-prepared samples, b) Barrett-Joyner-Halenda (BJH) pore size distribution curves

Journal Name RSCPublishing

COMMUNICATION

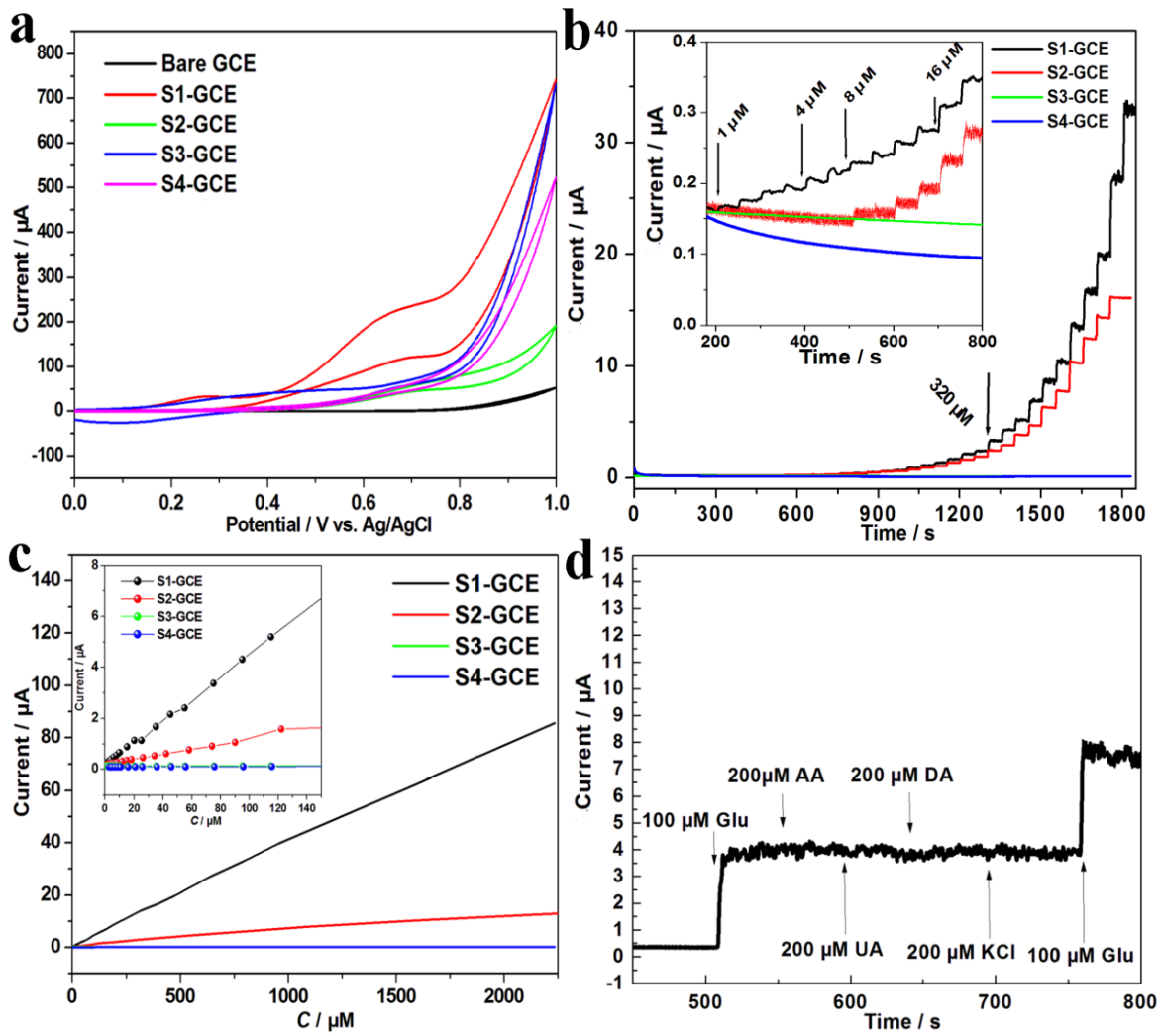

Figure 4 a) Cyclic voltammograms of the bare GCE, S1-GCE, S2-GCE, S3-GCE, and S4-GCE in 0.1 M NaOH with 5 μM glucose at a scan rate of 50 mVs^{-1}, b) Current–time responses at a potential of 0.60 V after successive injections of different amounts of glucose into stirring 0.1 M NaOH electrolyte, c) Plot of electrocatalytic current of glucose versus its concentrations from 0.125 to 2250 μM, (in inset, 0.125~150 μM), and d) Amperometric response of modified electrodes with successive addition of 100 μM glucose, 200 μM AA, 200 μM UA, 200 μM DA, 200 μM KCl and 100 μM glucose in 0.1 M NaOH solution, obtained on S1-GCE.

Gas sorption properties of $[Cu_3(btc)_2]$ with different morphologies are also studied. N_2 adsorption and desorption isotherms of the samples with different morphologies are shown in **Figure 3a**. All the samples show a characteristic Type I sorption isotherm, which is typical for mesoporous materials with high amounts of nitrogen adsorption. The S1 has the highest BET surface of 1398 m^2 g^{-1}, which indicates an excellent BET surface of mesoporous $[Cu_3(btc)_2]$ crystals and the value is close to the reference 30-$[Cu_3(btc)_2]$ nanocubes. The samples S2 and S3 have BET surfaces of 1342 and 1220 m^2 g^{-1}, and S4 has the smallest BET surface of 973m^2 g^{-1}, indicating that both additions of CTAB and different morphologies have a significant effect on the gas adsorption property. The hysteresis loops in the isotherms suggest the presence of mesopores in all four samples, as further shown in the Barrett-Joyner-Halenda (BJH) pore size distribution curves (**Figure 3b**). The average pore diameter of all the samples is around 4 nm, obviously, S1 has the largest pore volume of all. It is well known that mesopores play a critical role in electrochemical processes, due to their capability of facilitating

mass diffusion/transport (e.g., electrolyte penetration, and guest molecule/ion transport) and ensuring a high electroactive surface area. Therefore, different porous textures of the four samples are likely to affect their performance in electrochemical applications.

To make a comparison of the as-prepared samples, their electrochemical character was studied. Four $[Cu_3(btc)_2]$ nanostructures were modified onto the GC electrode, respectively, preparing different modified electrodes. **Electronic Supporting Information (ESI) Figure 1** exhibits the electrochemical impedance spectroscopies of the different modified electrodes. As shown in ESI Figure 1, after the $[Cu_3(btc)_2]$ nanomaterials, including bare GCE, S1, S2, S3 and S4 being modified onto the GC electrode. The impedance changes of the modification process show that $[Cu_3(btc)_2]$ nanomaterials had attached to the electrode surface. At the same time, the charge-transfer-R_{ct} is different when different nanomaterials are modified onto the GC electrode. As **ESI Table 1** shows, the order of R_{ct} is: S4-GCE > S3-GCE > S2-GCE > S1-GCE. That means, the electron transfer resistance is S1-GCE < S2-GCE < S3-GCE< S4-GCE, which also means the electron transfer ability is S1-GCE >S2-GCE > S3-GCE > S4-GCE.

Copper based electrodes are often considered in the same way as nickel electrodes with respect to organic molecule electrooxidation. They can catalyze oxidation by reducing the M(III) centre to M(II) (where M = Ni or Cu), however a distinct redox couple for the Cu(II)/(III) surface process is not clearly evident as it is for most nickel electrodes.[31-34] **Figure 4**a shows cyclic voltammetry responses of Bare-GCE, S1-GCE, S2-GCE, S3-GCE, and S4-GCE in 0.1 M NaOH solution, in the presence of 5 μM glucose, at a scan rate of 50 mVs^{-1}. There is a remarkable increase in the current of the S1-GCE after the addition of 5 μM glucose, with reference to the peak current of the modified electrode before its addition. Current-time responses at a potential of 0.60 V after successive injections of different amounts of glucose into stirring 0.1 M NaOH are shown in Figure 4b for S1-GCE, S2-GCE, S3-GCE, and S4-GCE, respectively. It can be seen from the inset of Figure 4b that S1-GCE displays a sensitive increase in current response after successive additions of glucose compared with other electrodes (even the addition of glucose solution is 1.0 μM). Such excellent catalytic activity of S1-GCE may be attributed to the synergistic nanoporous $[Cu_3(btc)_2]$ nanocubes, which includes high catalytic active sites for the glucose provided by the well-distributed nanocubic nanostructures and nanopores on the MOF unit. Additionally, high electrolyte penetration and guest glucose transport rates have been provided by an efficient surface area. What's more, plots of electrocatalytic current of glucose versus its concentrations from 0.125 μM to 2.25 mM glucose are shown in Figure 4c, and the linear equation of S1-GCE: $I(\mu A)=0.6739+38.8C(mM)$, R=0.9994 for S1-GCE, and the calculated sensitivity of 549 $\mu AmM^{-1}\ cm^{-2}$. Compared with other three modified electrodes, the calculated sensitivity and R are as follows: [77 $\mu AmM^{-1}\ cm^{-2}$, 0.9907 (S2-GCE)], [<1 $\mu AmM^{-1}\ cm^{-2}$, 0.9869 (S3-GCE)], and [<1 $\mu AmM^{-1}\ cm^{-2}$, 0.9855 (S4-GCE)] respectively. The sensitivity further proves the excellent electrocatalytic glucose oxidation of $[Cu_3(btc)_2]$ nanocubes.

One of the major challenges in nonenzymatic glucose detection is to eliminate the electrochemical response generated by some easily oxidizable endogenous interfering compounds such as ascorbic acid (AA), uric acid (UA), dopamine (DA), and KCl. In the physiological sample, the glucose concentration (3–8 mM) is generally much higher response than that of interfering species of AA (0.2 mM), UA (0.2 mM), DA (0.2 mM), and KCl (0.2 mM). Nevertheless, these interfering species can produce the oxidation current comparable to that of glucose, attributing to their higher electron transfer rates. It is expected that the $[Cu_3(btc)_2]$ nanocube modified electrode with a high active surface pots can favor a kinetically controlled sluggish reaction (the oxidation of glucose) to a greater extent than diffusion controlled reactions (the oxidation of interfering species). To verify this, we investigated the amperometric responses of S1-GCE, S2-GCE, S3-GCE and S4-GCE at an applied potential of +0.6 V in 0.1 M NaOH solution with continuous additions of 100 μM glucose, 200 μM AA, 200 μM UA, 200 μM DA and 200 μM KCl. Compared with the other four interfering species, a remarkable glucose signal is obtained from the current response in Figure 4d, **ESI Figure 2-4**. Compared to glucose, the interfering species yielded current response for S1-GCE ranging from <0.1% (AA), <0.1% (UA), 0.1% (DA), to 0% (KCl), while those of other electrodes (S2-GCE, S3-GCE and S4-GCE) show the interfering current signal obviously. These results indicate the $[Cu_3(btc)_2]$ nanocubes could be used for the selective and sensitive detection of glucose with negligible interference from AA, UA, DA and KCl. What's more, in **ESI Figure 5**, the curve is the stability of the response current for S1-GCE electrode after the addition glucose solution (320 μM) during 3200 seconds. It is seen that there is only 15.8% loss after 3200 seconds, which is stable enough to the application for the electrochemical sensor of glucose.

The performance of the as-prepared $[Cu_3(btc)_2]$ nanocubic electrocatalyst is compared with some of existing nonenzymatic sensors, as is shown in **ESI Table 2**. Clearly, the sensitivity or linear range of the S1 catalyst ($[Cu_3(btc)_2]$ nanocubes) is better than some other materials, such as Cu nanobelt (0.0798 μAmM^{-1}, 0.01~1.13 mM), [35] Cu implanted BDD (1.0~5.0 mM), [36] Cu nanoporous (220 μAmM^{-1}, 0.01~0.5 mM), [37] Cu wire (37.9 μAmM^{-1}, 0.01~1.0 mM), [38] Cu-BDD electrode (2.3 μAmM^{-1}), [39] Cu nps/SWCNTs/GC (0.256 μAmM^{-1}), [40] N-doped Carbon-Cu nanohybrids (223.6 μAmM^{-1}, 5 $\times 10^{-3}$~2.1 mM) [41] and so on. However, the sensitivity or linear range of some novel materials is better than our results, such as CuO/Cu electrode (761.9 μAmM^{-1}). [34] It can be concluded that the as-prepared $[Cu_3(btc)_2]$ nanocube catalyst is among the middle-top list of sensors with a good sensitivity, a fast response speed, and a low detection limit.

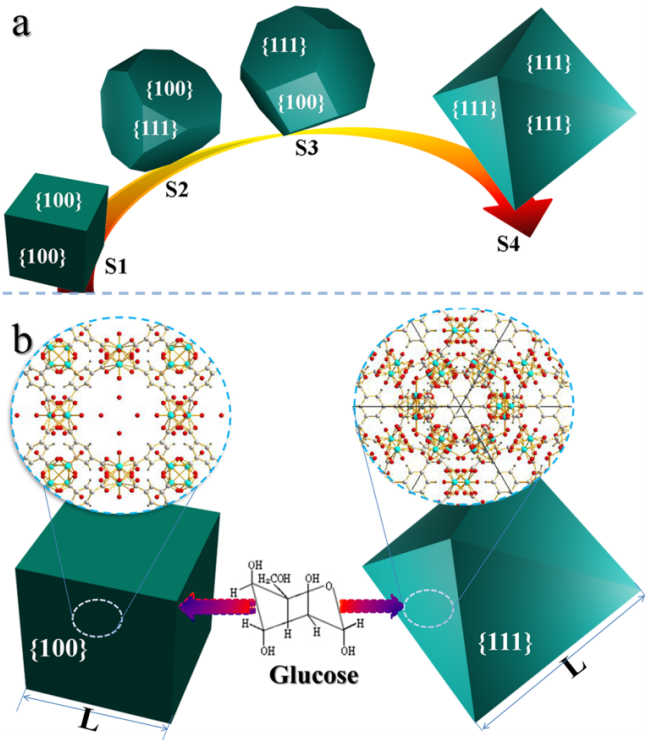

Figure 5 a) A scheme of crystal plane transformation from S1 to S4, b) The possible glucose diffusion in {001} or {111} crystal planes, **L**=the glucose diffusion length.

These superiorities are believed to be due to several reasons, such as: 1) The specific surface-interface of copper metal-organic framework nanocrystal plane (Seen **Figure 5** and **ESI Figure 6**, **7**). From Figure 5a, it is seen that {100} crystal planes decrease while {111} crystal planes increase from cubes to octahedrons. In ESI Figure 6, it is shown that there is a typical nanopore on the {100} crystal planes, while not any nanopore can be seen on the {111} crystal planes in ESI Figure 7. Then the nanocubic crystal-S1 with 6 {100} facets can enhance the electrocatalytic activity due to the typical nanopores on the {100} crystal planes for the guest-glucose diffusion in Figure 5b. With the decrease of the {100} crystal plane and increase of the {111} crystal plane from S1 to S4, the guest-glucose diffusion become difficult, thus the electrocatalytic activity towards glucose has decreased from S1 to S4. On the other hand, the glucose diffusion in host materials is associated with the glucose diffusion coefficient and the diffusion length (**L**) in Figure 5b. As we know, the glucose diffusion coefficient depends on the instinct of the host materials. Therefore, minimizing the particle size to shorten the glucose diffusion length is an effective strategy to enhance the capability of electrocatalytic activity. $[Cu_3(btc)_2]$ nanocubes with porous {100} crystal planes have the largest surface area and the smallest size of all the samples, which can effectively shorten the glucose transport length and enhance the electrochemical response for the glucose.

Conclusions

In summary, $[Cu_3(btc)_2]$ with different nanostructures has been firstly described as nonenzymatic electro-catalysts for the glucose. Especially, the obtained $[Cu_3(btc)_2]$ nanocube with porous 6 {100} facets modified electrode shows the best nonenzymatic electro-catalytic glucose activity among the four as-prepared samples. The nonenzymatic electro-catalytic glucose activity decreases as the morphology of the $[Cu_3(btc)_2]$ nanocrystals change from the cube to the octahedron. In addition, the $[Cu_3(btc)_2]$ nanocube modified electrode exhibits high nonenzymatic electrocatalytic activity for glucose in basic conditions with high sensitivity, low detection limit, and excellent selectivity. Thus, the $[Cu_3(btc)_2]$ nanocubes hold the great potential for the development of nonenzymatic glucose sensors.

Experimental section

Agents: benzene-1,3,5-tricarboxylate, cupric nitrate, sodium hydroxide, glucose and all other chemicals were obtained from Beijing Chemical Factory and used as received. Unless otherwise stated, water used throughout all experiments was purified with the Millipore system (18.2 MΩ cm).

Synthesis of $[Cu_3(btc)_2]$ nanocrystals: $[Cu_3(btc)_2]$ nanocrystals have been prepared by a modified method of Sun et al.[30] In a typical experiment, the surfactant of CTAB (0-25 mmol) was dissolved in 50 mL of 1:1 (v/v) mixture of ethanol and deionized water and stirred vigorously for 5 mins at room temperature until a transparent solution was obtained. Then 0.15 mL of a 0.1 M $Cu(NO_3)_2$ aqueous solution and 0.1 mL of a 0.1 M btc sodium salt aqueous solution were added respectively and the reaction mixture was stirred vigorously for an additional 5 min at room temperature. The resulted blue green powder was isolated by centrifugation, washed with ethanol for 3 times and dried under vacuum for 5 h at room temperature. For a given concentration of CTAB (0, 0.005 M, 0.01 M, and 0.1 M, the corresponding product denoted by S1, S2, S3, and S4), only the concentration of reactants changes while other conditions like temperature, solvent, and reaction time remain unchanged.

Characterization: Scanning electron microscopy (SEM) was conducted by JEOL JSM-6701F field-emission scanning electron microscope (FE-SEM) for surface morphology observations. The phase analyses of the samples were performed by X-ray diffraction (XRD) on a Rigaku-Ultima III with Cu Ka radiation (λ= 1.5418 Å). Nitrogen adsorption–desorption measurements were performed on a Gemini VII 2390 Analyzer at 77 K using the volumetric method. The specific surface area was obtained from the N_2 adsorption–desorption isotherms and was calculated by using the Brunauer–Emmett–Teller (BET) method. Electrochemical experiments were performed on a CHI 660B electrochemical station (CHI Instruments Inc., Shanghai) with a conventional three-electrode system. The $[Cu_3(btc)_2]$ nanocrystal modified glassy carbon electrodes are used as the working electrode, respectively. A Pt wire and a saturated calomel electrode (SCE) acted as the counter and reference

electrodes, respectively. We have reproduced three times for each characterization.

Acknowledgements

This work is supported by the Program for New Century Excellent Talents of the University in China (grant no. **NCET**-13-0645) and National Natural Science Foundation of China (**NSFC**-21201010, U1304504), Program for Innovative Research Team (in Science and Technology) in University of Henan Province (**14IRTSTHN004**), the Science & Technology Foundation of Henan Province (14B150001, 122102210253, 13A150019), and the China Postdoctoral Science Foundation (2012M521115). We are very grateful to ***Liang Chen*** from Anyang Normal University in the language modification.

Notes and references

[a] *College of Chemistry and Chemical Engineering, Anyang Normal University, Anyang, 455002, Henan, P. R. China.*
[b] *State Key Laboratory of Coordination Chemistry, Nanjing University, Nanjing, 210093 Jiangsu, P. R. China.*
*E-mail: *huanpangchem@hotmail.com*
†Electronic Supplementary Information (ESI) available: [details of any supplementary information available should be included here]. See DOI: 10.1039/c000000x/

1. Y. Fu, D. Sun, Y. Chen, R. Huang, Z. Ding, X. Fu and Z. Li, *Angew. Chem. Int. Ed.*, 2012, 51, 3364.
2. L. T. L. Nguyen, T. T. Nguyen, K. D. Nguyen and N. T. S. Phan, *Applied Catalysis A: General* 2012, 44, 425–426.
3. M. Jahan, Q. Bao and K. P. Loh, *J. Am. Chem. Soc.*, 2012, 134, 6707.
4. L. L. Wen, F. Wang, J. Feng, K. L. Lv, C. G. Wang and D. F. Li, *Cryst. Growth Des.*, 2009, 9, 3581.
5. F. Luo, Y. X. Che and J. M. Zheng, *Cryst. Growth Des.*, 2009, 9, 1066.
6. B. Zheng, R. Yun, J. Bai, Z. Lu, L. Du and Y. Li, *Inorg. Chem.*, 2013, 52, 2823.
7. L. E. Kreno, K. Leong, O. K. Farha, M. Allendorf, R. P. Van Duyne and J. T. Hupp, *Chem. Rev.*, 2012, 112, 1105–1125.
8. F. Sun, Z. Yin, Q. Q. Wang, D. Sun, M. H. Zeng and M. Kurmoo, *Angew. Chem. Int. Ed.*, 2013, 52, 4538–4543.
9. M. M. Wanderley, C. Wang, C. D. Wu and W. B. Lin, *J. Am. Chem. Soc.* 2012, 134, 9050−9053.
10. C. M. Doherty, D. Buso, A. J. Hill, S. Furukawa, S. Kitagawa and P. Falcaro, *Acc. Chem. Res.* 2014, DOI: 10.1021/ar400130a.
11. W. J. Ma, Q. Jiang, P. Yu, L. F. Yang and L. Q. Mao, *Anal. Chem.* 2013, 85, 7550−7557.
12. J. Mao, L. Yang, P. Yu, X. W. Wei and L. Q. Mao, *Electrochem. Commun.*, 2012,19, 29.
13. C. Y. Zhang, M. Y. Wang, L. Liu, X. J. Yang and X. Y. Xu, *Electrochem. Commun.,* 2013, 33, 131–134.
14. H. Hosseini, H. Ahmar, A. Dehghani, A. Bagheri, A.Tadjarodi and A. R. Fakhari, *Biosens. Bioelectron.*, 2013, 42, 426–429.
15. H. Hosseini, H. Ahmar, A. Dehghani, A. Bagheri, A. R. Fakhari and M. M. Amini, *Electrochim. Acta*, 2013, 88, 301–309.
16. S. B. Wang, Y. D. Hou, S. Lin and X. C. Wang, *Nanoscale*, 2014, DOI: 10.1039/C4NR02399D.
17. J. Wang, H. Pang, J. Yin, L. Guan, Q. Lu and F. Gao, *CrystEngComm*, 2010, 12, 1404-1409.
18. L. H. Hu, Q. Peng and Y. D. Li, *J. Am. Chem. Soc.*, 2008, 130, 16136-16137.
19. H. Pang, J. W. Deng, J. M. Du, S. J. Li, J. Li, Y. Ma, J. Zhang and J. Chen, *Dalton Trans.*, 2012, 41, 10175-10181
20. Y. Fan, R. Liu, W. Du, Q. Lu, H. Pang and F. Gao, *J. Mater. Chem.*, 2012, 22, 12609-12617.
21. H. Pang, Y. C. Li, L. N. Guan, Q. Y. Lu and F. Gao, *Catal. Commun.*, 2011, 12, 611-615.
22. S. S.-Y. Chui, S. M.-F. Lo, J. P. H. Charmant, A. G. Orpen and I. D. Williams, *Science*, 1999, 283, 1148.
23. M. Schlesinger, S. Schulze, M. Hietschold and M. Mehring, *Microporous Mesoporous Mater.*, 2010, 132, 121.
24. Z.-Q. Li, L.-G. Qiu, T. Xu, Y. Wu, W. Wang, Z.-Y. Wu and X. Jiang, *Mater. Lett.*, 2009, 63, 78.
25. Y. K. Seo, G. Hundal, I. T. Jang, Y. K. Hwang, C. H. Jun and J. S. Chang, *Microporous Mesoporous Mater.*, 2009, 119, 331.
26. H. Yang, S. Orefuwa and A. Goudy, *Microporous Mesoporous Mater.*, 2011, 143, 37.
27. A. Umemura, S. Diring, S. Furukawa, H. Uehara, T. Tsuruoka and S. Kitagawa, *J. Am. Chem. Soc.*, 2011, 133, 15506.
28. Z. Ni and R. I. Masel, *J. Am. Chem. Soc.*, 2006, 128, 12394.
29. J.-L. Zhuang, D. Ceglarek, S. Pethuraj and A. Terfort, *Adv. Funct. Mater.*, 2011, 21, 1442.
30. Q. Liu, L.-N. Jin and W.-Y. Sun, *Chem. Commun.*, 2012, 48, 8814–8816.
31. P. Luo, S. V. Prabhu and R. P. Baldwin, *Anal. Chem.* 1990, 62, 752 – 755.
32. F. Sun, L. Li, P. Liu and Y. F. Lian, *Electroanal.* 2011, 23, 395 –401.
33. H. X. Wu, W. M. Cao, Y. Li, G. Liu, Y. Wen, H. F. Yang and S. P. Yang, *Electrochim.Acta* 2010, 55, 3734 –3740.
34. J. A. Yang, W. D. Zhang and S. Gunasekaran, *Biosens. Bioelectron.* 2010, 26, 279– 284.
35. H. F. Cui, J. S. Ye, W. D. Zhang, C. M. Li, J. H. T. Luong and F. S. Sheu, *Anal. Chim. Acta*., 2007, 594, 175–183.
36. T. Huang, K. Lin, S. Tung, T. Cheng, I. Chang, Y. Hsieh, C. Lee and H. Chiu, *J. Electroanal Chem.,* 2009, 636, 123–127.
37. T. Watanabe, T. A. Ivandini, Y. Makide, A. Fujishima and Y. Einaga, *Anal. Chem.,* 2006, 78, 7857–7860.
38. S. Sattayasamitsathit, P. Thavarungkul, C. Thammakhet, W. Limbut, A. Numnuam, C. Buranachai and P. Kanatharana, *Electroanalysis.,* 2009, 21, 2371–2377.
39. Z. L. Chen and D. B. Hibbert, *J Chromatogr. A.*, 1997, 766, 27–33.
40. T. You, O. Niwa, Z. Chen, K. Hayashi, M. Tomita and S. Hirono, *Anal. Chem.*, 2003, 75, 5191–5196.
41. C. Z. Wei, Y. Y. Liu, X. R. Li, J. H. Zhao, Z. Run, and H. Pang, *ChemElectroChem*, 2014, 1, 799-807.

ToC

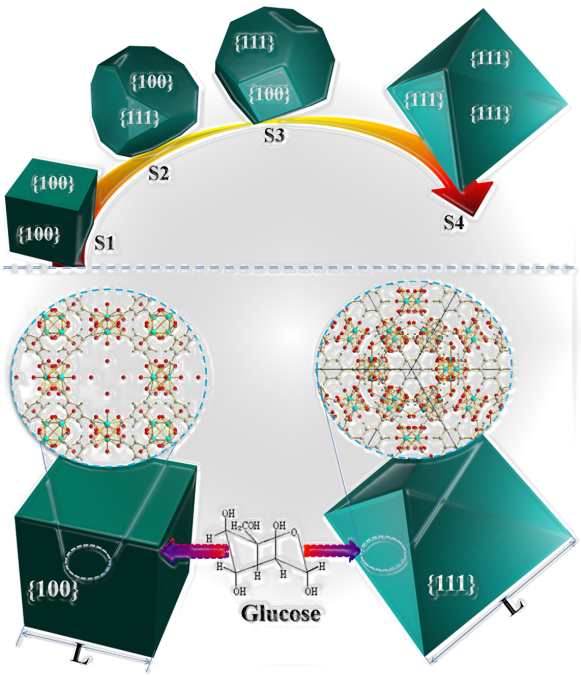

Nanocrystal plane affects nonenzymatic electro-catalytic glucose of $[Cu_3(btc)_2]$ nanocrystals, and the activity changes from the high sensitive to general with the decreasing of {100} crystal planes from cubes to octahedra.